



Enhanced Light Absorption and Charge Carrier Management in Core-Shell Fe₂O₃@Nickel Nanocone Photoanodes for Photoelectrochemical Water Splitting

Ashutosh K. Singh^{+,*}[a] and Debasish Sarkar^{+,*}[b, c]

Solar driven photoelectrochemical (PEC) water splitting is a clean and sustainable approach to generate green fuel, Hydrogen. Hematite (Fe₂O₃) is considered as potential photoanode because of its abundance, chemical stability and suitable band gap, though its short carrier diffusion length puts a limit on the film thickness and subsequent light absorption capability. In this regard, here we have designed and constructed a unique photoanode by depositing ultrathin films of Fe₂O₃ on purpose-built three-dimensional (3D) nickel nanocone arrays. In this design, 3D nanostructures not only provide ameliorated surface area for PEC reactions but also enhance light absorption capability in ultrathin Fe₂O₃ films, while ultrathin films promote

charge carrier separation and effective transfer to the electrolyte. The 3D electrodes exhibit a substantial improvement in light absorption capability within the entire visible region of solar spectrum, as well as enhanced photocurrent density as compared to the planar Fe₂O₃ photoelectrode. Detailed investigation of reaction kinetics suggests an optimum Fe₂O₃ film thickness on 3D nanocone arrays obtained after 6 deposition cycles in achieving maximum charge carrier separation and transfer efficiencies (82% and 88%, respectively), mainly ascribable to the increased charge carrier lifetime overcoming recombination losses.

1. Introduction

Exorbitant consumption of fossil fuels to meet global energy demand and subsequent concerns over raising environment pollution make green and renewable fuels production increasingly indispensable.^[1–3] Among various fuel candidates, Hydrogen (H₂) is considered to be the most-potent and next-generation energy carrier because it has zero carbon footprint and high in energy density.^[2] In this regard, solar-driven photoelectrochemical (PEC) water splitting is the cleanest and most effective technique for harnessing and storing solar energy in the form of chemical bonds.^[1,2,4] Since its invention in 1972, a host of metal oxides have been explored as efficient

catalysts for PEC water splitting. Among these, hematite (Fe₂O₃) has drawn particular attention as a promising photo-electrode material because of its suitable band gap for significant light absorption in the visible region of the solar spectrum, high abundance and astounding chemical stability in aqueous electrolytes.^[4–7] However, it's performance is critically limited by a very short hole diffusion length (~2–4 nm) and poor majority carrier conductivity which lead to recombination losses of photogenerated charge carriers in the bulk.^[4,5,7] This limitation can be overcome by designing customized nanostructures of hematite, modifying their electronic structure via doping, and also by including co-catalysts.^[4,5,8]

Indeed, nanostructuring process allows significant enhancement in the relative volume of space-charge region as compared to that in bulk, while maintaining sufficient material for complete light absorption.^[6] Moreover, rational designing and fabrication of hybrid mesostructures are also found effective in enhancing the photocurrent density of hematite based photoanodes, though far less than its ideal photocurrent density.^[4,7,9] Most of these studies are mainly focused on the nano-morphology of the PEC active material ('guest') itself and less attention has been paid on the development of 3D nanostructured 'host'.^[5] Thinning down of PEC active 'guest' material would definitely reduce carrier diffusion length and subsequent recombination losses, but it also reduces the light absorption capability of the active material. Interestingly, this situation can be handled by developing 3D ordered nanophotonic structures for sufficient light absorption with a very small amount of PEC active material.^[4,5] Such a design strategy not only improves the specific surface area of the active material but also promotes trapping of incident radiation in the near surface region for bettered light absorption.^[4,9] In this


[a] Dr. A. K. Singh⁺
Large Area Device Laboratory
Centre for Nano and Soft Matter Sciences
Bengaluru-560013 (India)
E-mail: aksingh@cens.res.in
ashuvishen@gmail.com

[b] Dr. D. Sarkar⁺
Solid State and Structural Chemistry Unit
Indian Institute of Science
Bengaluru-560012 (India)
E-mail: deb.sarkar1985@gmail.com

[c] Dr. D. Sarkar⁺
Department of Physics
Malaviya National Institute of Technology Jaipur
Jaipur, Rajasthan-302017 (India)
E-mail: debasish.phy@mnit.ac.in

[⁺] Authors contributed equally to this work.

 Supporting information for this article is available on the WWW under <https://doi.org/10.1002/cctc.201901836>

 This manuscript is part of the Special Issue "Photocatalysis: From Solar Power to Sustainable Chemical Production", which is part of the wider project "Building A New Energy Economy with Catalysis".

regard, thinning down of hematite layer deposited on these 3D photonic structures to the level comparable to its hole diffusion length would facilitate charge carrier separation and subsequent transfer probability without sacrificing sufficient light absorption capability of the whole 'host-guest' system. This scheme of electrode designing thus meets the requirement of optically 'thick' and 'electrically 'thin' materials for enhanced PEC performance.^[4]

Here, we have demonstrated an efficient technique for PEC water splitting by ultrathin Fe_2O_3 films deposited on regular arrays of 3D nickel (Ni) nanocone (NC) arrays. The NC arrays are fabricated using one-step electrodeposition technique without using any template, which is relatively easy and straightforward as compared to lithography and other template assisted methods used for developing 3D nanophotonic structures.^[5] In this structure, the purpose-built Ni NC arrays have been utilized to harvest incident solar radiation efficiently over the whole visible region with the thin Fe_2O_3 layer used for sufficient charge carrier generation and carrying out the water splitting reactions at the electrode-electrolyte interface. To the best of our knowledge, this is the first ever report on design and development of Fe_2O_3 -Ni NC based core-shell nanostructured photoanodes for PEC water splitting.

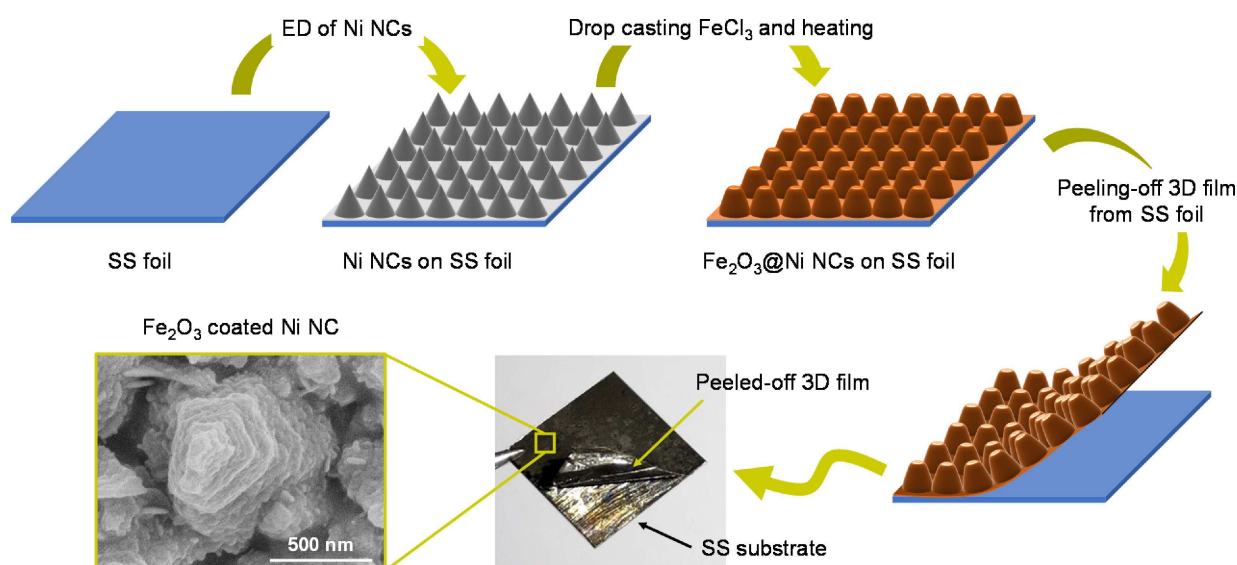
2. Results and Discussion

2.1. Morphological Investigation of 3D Fe_2O_3 /Ni NC Electrodes

The synthesis strategy of Ni NC arrays on SS substrate and subsequent decoration of Fe_2O_3 films in order to realize 3D Fe_2O_3 /Ni NC core-shell nanostructures is schematically presented in Scheme 1.

The electrodeposition process forms almost uniform and vertically oriented Ni NC arrays on the SS substrate. We have

also deposited Ni NCs on various other substrate materials including Ni foam and Ni plates, suggesting versatility of this electrodeposition technique in growing ordered Ni NC arrays on a large scale (Figure S1, Supplementary Information) irrespective of the nature of the substrate. Such growth technique under certain conditions including deposition voltage, current and electrolyte temperature also ensure reproducible nanostructure formation without aggregation. Ultrathin films of Fe_2O_3 is then deposited on to the surface of these NCs and act as the electroactive material of the hybrid electrode. The Fe_2O_3 coated Ni NCs thin film is then easily peeled off from the SS substrate to get a highly-flexible and free-standing 3D Fe_2O_3 /Ni NC core-shell nanostructured electrode. This easy peeling-off was possible presumably because of the surface oxidation layer of commercial SS foil making the adhesion between Ni NCs and SS foil weak. The morphology of pristine Ni NC arrays (top view) observed through FESEM is depicted in Figure 1a and suggests that the NCs grow almost vertically over the substrate along with the coexistence of larger and smaller cones. The base of the NCs has an average diameter of 400 nm and mean height of the NCs is measured about 1–2 μm . The NCs are very sharp tipped with a distance of about 400–600 nm between them, while the surface of the NCs is rough and would be advantageous for anchoring Fe_2O_3 nanoparticles tightly. XRD pattern of these NCs (Figure S2, Supplementary Information) shows three prominent diffraction peaks in accordance with the standard pattern (JCPDS No. 04-0850) of face-centered cubic (fcc) phase of Ni.^[5] Few additional peaks in the diffraction pattern can be ascribed to the reflections from the SS substrate. Surface of the Ni NCs becomes rougher after the deposition of Fe_2O_3 nanoparticles, as can be observed in Figures 1b–c, for 3 and 6 cycles of Fe_2O_3 deposition. Such rough surface morphology of the electrodes would be beneficial for providing ameliorated PEC reaction sites for bettered performance. However, the surface morphology of hybrid NCs obtained after



Scheme 1. Schematic illustration of fabricating Fe_2O_3 coated Ni NC arrays electrodeposited on SS foil.

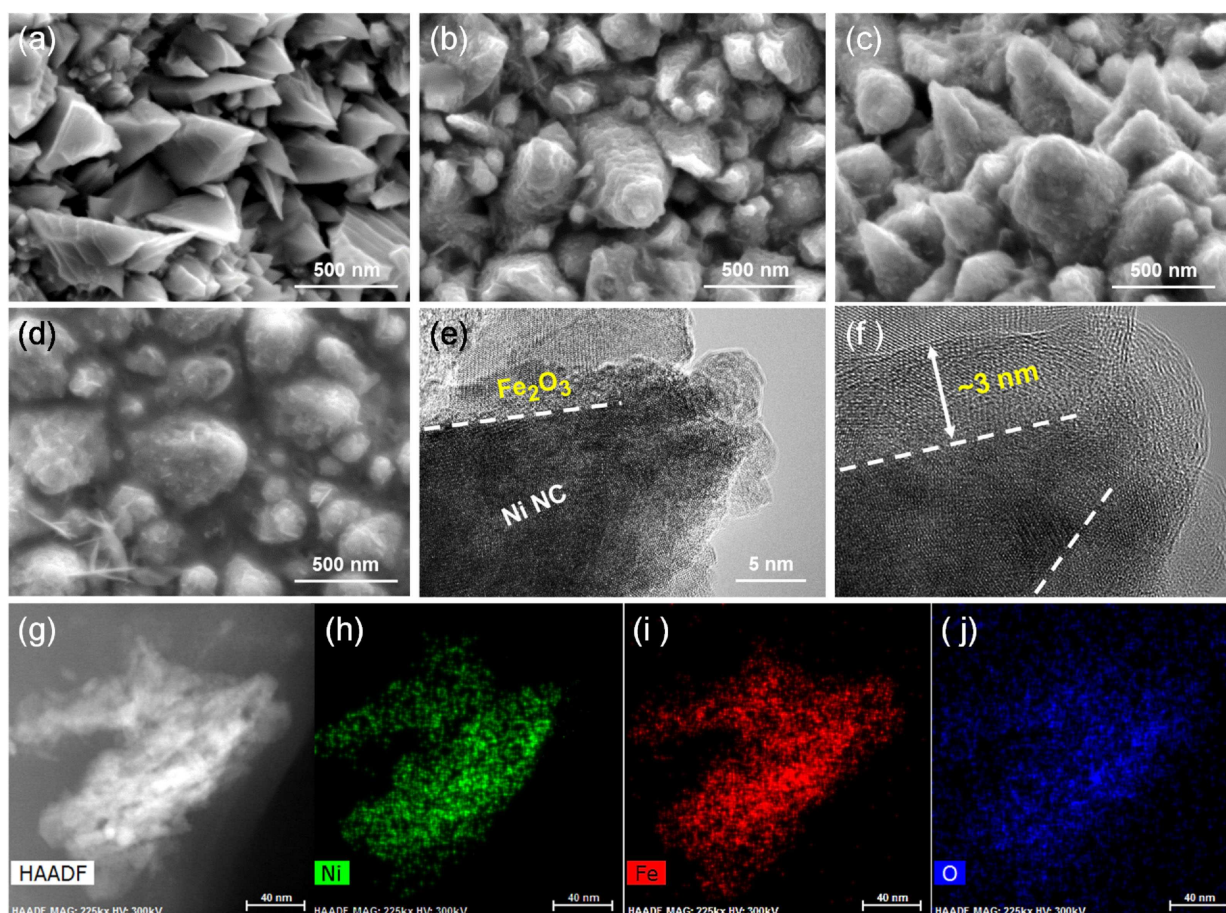


Figure 1. (a) FESEM image of pristine Ni NC arrays electrodeposited on SS substrate; surface morphology of Fe_2O_3 coated Ni NC arrays after (b) 3 deposition cycles, (c) 6 deposition cycles and (d) 10 deposition cycles; (e) shows the TEM image of a single Fe_2O_3 coated Ni NC obtained after 6 deposition cycles; (f) corresponding high-resolution TEM image showing Fe_2O_3 coating over Ni NC; (g) HAADF-STEM image of an individual Fe_2O_3 coated Ni NC and (h)–(j) show the EELS color mapping of various constituent elements of the hybrid NC.

10 cycles of Fe_2O_3 deposition looks relatively smoother (Figure 1d) as compared to other two. Top views also suggest that the morphology of hybrid electrode materials is composed of densely-packed regular NCs with dome shapes at the top, indicating complete coverage of Ni NCs with Fe_2O_3 nanoparticles. EDS color mapping of individual elements (Figure S3, Supplementary Information) further suggests a uniform covering of Fe_2O_3 nanoparticles over vertically grown Ni NC arrays. These hybrid nanostructures are further investigated through TEM and high resolution TEM as shown in Figures 1e and f, respectively, for the Fe_2O_3 coated Ni NCs sample obtained after 6 deposition cycles. Distinct differences in contrasts can be observed on moving from the center to the edges of the Fe_2O_3 coated NCs, suggesting the formation of core-shell type nanostructures. However, the thickness of the Fe_2O_3 thin film is not uniform, in accordance with the rough surface morphology observed through FESEM, and varies within 2–5 nm, as can be observed clearly from Figures 1f and S4(a) (Supplementary Information). High resolution TEM image (Figure S4(b), Supplementary Information) also shows well resolved lattice fringes with separation of ~ 0.25 nm which matches well with the interplanar spacings of (110) lattice planes of rhombohedral

Fe_2O_3 .^[7,10,11] Figure 1g shows the scanning TEM (STEM) image where the contrast difference between core and shell regions of the NC can be further identified. Finally, the elemental mapping micrographs (Figures 1h–j) for a single $\text{Fe}_2\text{O}_3/\text{Ni}$ hybrid NC obtained through electron energy loss spectrometry (EELS) suggest uniform covering of Fe_2O_3 over 3D Ni NC.

Now, to substantiate the chemical nature of Fe in deposited iron oxide, $\text{Fe}2p$ core level XPS spectra are recorded for all three 3D samples and analyzed as shown in Figure 2a and Figure S5 (Supplementary Information). The $\text{Fe}2p_{3/2}$ and $\text{Fe}2p_{1/2}$ peaks for all the samples are centered around binding energies 711 eV and 725 eV, respectively, which are typical values for Fe^{3+} in Fe_2O_3 and Fe_3O_4 , and are not compatible with that for FeO .^[12,13] A satellite peak of the $\text{Fe}2p_{3/2}$ main line can also be identified at ~ 719 eV, which further substantiates the presence of Fe^{3+} species.^[12,13] Interestingly, the $\text{Fe}2p$ spectra also exhibit a satellite peak ~ 716 eV which corresponds to the Fe^{2+} species and can be attributed to the presence of oxygen vacancies (V_{O}) generated during heat treatment in Ar atmosphere.^[12,14] To further characterize the as prepared Fe_2O_3 films, all 3D, as well as planar Fe_2O_3 samples are analyzed with Raman spectroscopy and spectra are shown in Figure 2b. All spectra exhibit

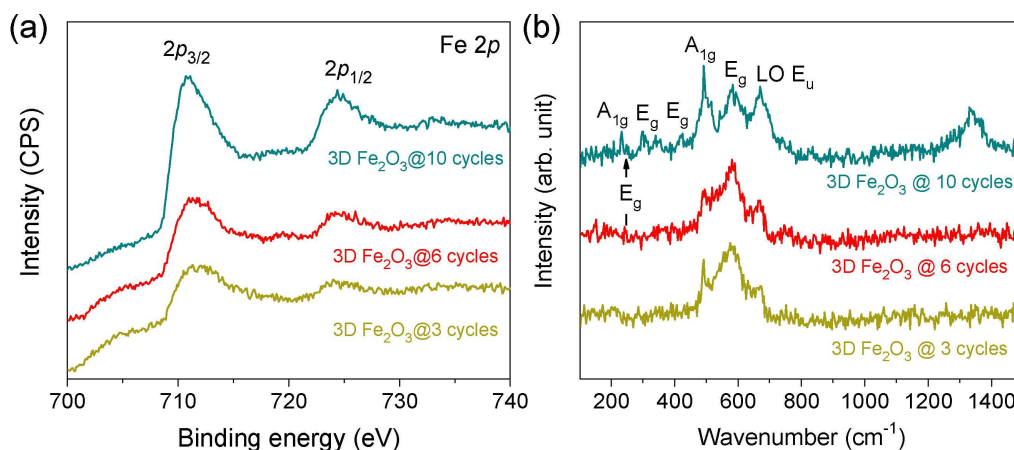


Figure 2. (a) Fe2p core level XPS spectra obtained from all three 3D Fe₂O₃ coated Ni NC samples; (b) Room temperature Raman spectra of all three 3D samples.

characteristic bands of Fe₂O₃, like A_{1g} (230 and 492 cm⁻¹), E_g (242, 297, 425, 590 cm⁻¹) and two-magnon scattering bands (~1330 cm⁻¹),^[15,16] The peak around 670 cm⁻¹ generally observed in Fe₂O₃ Raman spectra is reported to be originated from some small magnetite inclusion in the films or some disorder present in the Fe₂O₃ crystal lattice.^[16] However, as also indicated in XPS analysis, the presence of oxygen vacancy related disorder could be the best possible interpretation of the band around 670 cm⁻¹ in the Raman spectra.^[16,17]

2.2. Electrochemical Characterization of the Electrodes

Optical properties of all electrode materials are investigated because of their primary importance in efficient PEC water splitting process. Figure 3a depicts the digital photographs of the planar Fe₂O₃ and 3D Fe₂O₃/Ni NC electrodes for comparison. It is interesting to note that the 3D electrode is much darker as compared to the planar electrode, suggesting significantly enhanced light absorption capability owing to the 3D nano-

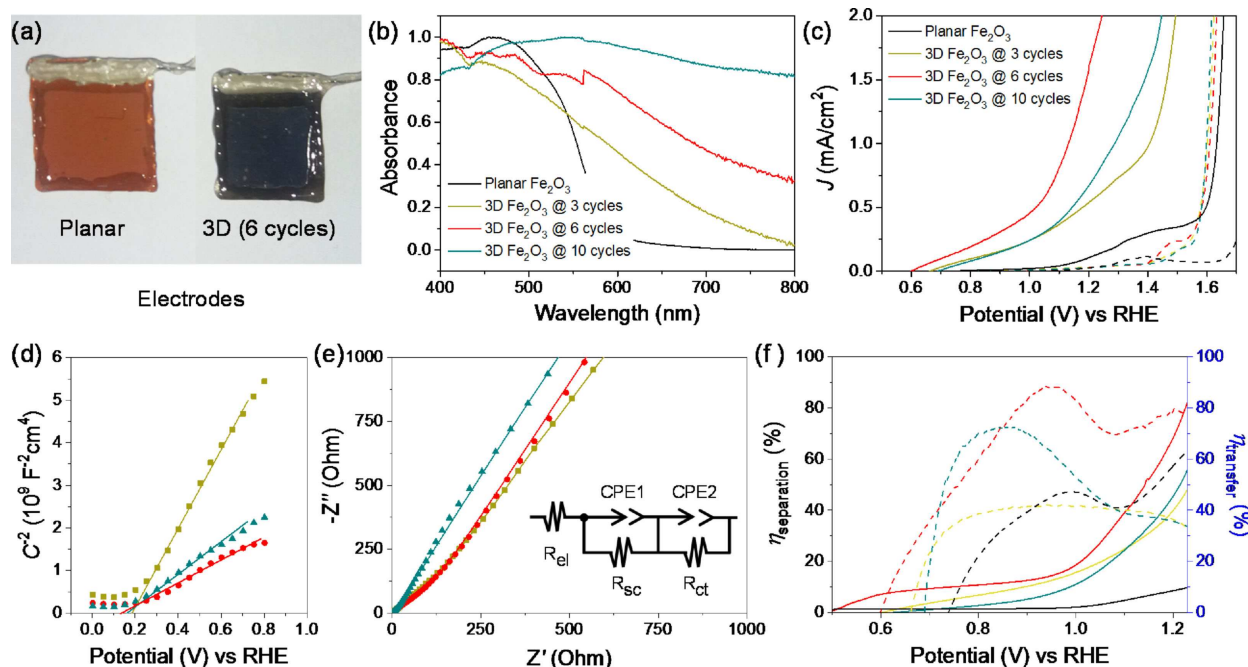


Figure 3. (a) Digital photographs of planar and 3D electrodes comparing their light absorbing capability; (b) absorption spectra of all electrodes within the visible region of electromagnetic spectrum; (c) current density (*J*) vs. potential (*V*) curves for the planar and 3D electrodes in the dark (dashed lines) and under solar irradiation (solid lines); (d) Mott-Schottky plots of the 3D electrodes obtained at an AC field frequency of 10 kHz under lighting condition; (e) comparison of Nyquist plots of all 3D electrodes under simulated sunlight (scattered data points), inset shows the equivalent circuit model used for fitting the Nyquist plots (solid lines); and (f) comparison of charge separation efficiency ($\eta_{\text{separation}}$) (solid lines) and charge transfer efficiency (η_{transfer}) (dashed line) of the photoelectrodes under 100 mW/cm² AM 1.5G illumination.

structured electrode design. This argument is further validated through UV-visible optical absorption spectroscopy of the electrode materials recorded using an integrating sphere and spectra are shown in Figure 3b. Planar Fe₂O₃ shows an absorption threshold around 597 nm, corresponding to an optical band gap of ~2.1 eV, which matches well with the results reported in literatures.^[6,15,18] Indeed, the Fe₂O₃ deposited 3D electrodes show much better light absorption as compared to the planar one, especially towards the longer wavelength region, indicating strong light trapping effect by the 3D nanostructure. The average distance between neighboring Fe₂O₃ coated Ni NCs are within 400–600 nm, comparable to the wavelengths of incident light, thus enhances the diffraction effect to enhance light absorption capacity, as usually observed for 3D photonic nanostructures.^[3–5] It is also interesting to note that increase in the thickness of Fe₂O₃ layer on 3D Ni NCs enhances absorption efficacy of longer wavelength radiations, envisaging the usefulness of these 3D nanostructured electrodes towards efficient PEC water splitting within full UV-visible region of solar spectrum.

Figure 3c demonstrates the PEC *J*-*V* curves of the planar and 3D Fe₂O₃ electrodes to evaluate the oxygen evolution reaction (OER) activities of the photoelectrodes. The polarization curves are measured for all the electrodes under dark and lighting conditions against Ag/AgCl reference electrode in 1 M NaOH aqueous electrolyte (pH ~ 13.6). Then, the potential scale (vs Ag/AgCl) is converted to the Reversible Hydrogen Electrode (RHE) scale according to the Nernst Equation [Eq. (1)] given as:^[4,7,8]

$$E_{RHE} = E + E_0 + 0.05916pH \quad (1)$$

where, E_{RHE} is the potential vs RHE, $E_0 = 0.1976$ V at 25 °C and E is the measured potential vs Ag/AgCl. For the planar electrode the photocurrent density is found to be very small (around 0.133 mA/cm² at 1.23 V vs RHE) owing to the low specific surface area and high surface recombination probability of photogenerated charge carriers. All of the 3D nanostructured electrodes exhibit significantly enhanced photocurrent density as compared to the planar electrode. It is interesting to observe that, with increasing Fe₂O₃ deposition cycles (from 3 to 6) photocurrent density increases and maximum photocurrent is observed for the 3D electrode obtained after 6 cycles of Fe₂O₃ deposition on Ni NCs, with the maximum photocurrent density of 1.86 mA/cm² at 1.23 V vs RHE. Here, it should be mentioned that with such current density values, this '3D Fe₂O₃@6 cycles' electrode outperforms many other Fe₂O₃ based photoelectrodes reported in recent literatures (Table S1, Supplementary information). However, the photocurrent density decreases with further increment in Fe₂O₃ deposition cycles (from 6 to 10). It is to be noted that the dark current for all the electrodes is negligible, indicating that the conductive Ni NC substrates have been well covered with the Fe₂O₃ film and hence it could be expected that the Fe₂O₃ films are solely responsible for the generation of photocurrent through water oxidation reactions. For some quantitative understanding of photoconversion efficiency (η) of the photoanodes (Equation S1, Supplementary Information), the '3D Fe₂O₃@6 cycles' electrode exhibits the highest efficiency

with $\eta \sim 0.1\%$ at ~1V vs RHE, which is double of the value for other 3D electrodes and almost 25 times more efficient than the planar electrode. From the *J*-*V* curves it can also be observed that the onset potential of photocurrent generation for the 3D nanostructured Fe₂O₃ electrodes varies within 0.6 to 0.7 V vs RHE, which is more cathodic than ~1 V, observed for the planar Fe₂O₃ electrode, indicating improved reaction kinetics or photocatalytic activity of the 3D hybrid electrodes and would be beneficial for solar decomposition of water at smaller potentials. Enhanced photocurrent density at higher potentials indicates a higher rate of delivery of electrons or holes at the electrode/electrolyte interface. Therefore, improved PEC performance of 3D nanostructured electrodes over their planar counterpart can be ascribed to the higher specific surface area of 3D substrates providing ameliorated reaction sites for water oxidation together with enhanced light harvesting capability owing to the light trapping effect of the 3D nanostructures. Additionally, increasing thickness of Fe₂O₃ layer over Ni NCs with increasing deposition cycles facilitate sufficient light absorption for charge carrier generation. As observed from the TEM investigation, the thickness of Fe₂O₃ film over Ni NCs is about 2–5 nm after 6 deposition cycles, comparable to the carrier diffusion length of minority carriers in Fe₂O₃, thus promote charge separation followed by their fast transfer into the electrolyte for water oxidation overcoming recombination losses. To validate the influence of light absorption on the PEC performance of photoanodes, the corresponding light harvesting efficiency (LHE) or light absorptance vs wavelength curves (Figure S6, Supplementary Information) are calculated according to Equation S2 (Supplementary Information), which again shows significantly improved LHE, especially in the longer wavelength regions, of the 3D nanostructured electrodes. Moreover, by integrating the absorptance curves with the standard solar spectrum, the unity converted photocurrent densities (J_{abs}) (Figure S7, Supplementary Information) are found to be significantly higher for the 3D electrodes in relation to the planar one (2.16 mA/cm² for the planar and 3.71 mA/cm² for '3D Fe₂O₃@6 cycles' electrodes, for instance). Therefore, such significantly enhanced photocurrent densities for the 3D photoelectrodes should be mainly ascribed to the enhanced bulk charge separation ($\eta_{separation}$) and surface charge transfer ($\eta_{transfer}$) efficiencies and will be elaborated later in the manuscript.^[19] However, with further increase in Fe₂O₃ film thickness (as in case of 3D films obtained after 10 deposition cycles), although there is an increase in light harvesting efficiency (Figure S7, Supplementary Information), higher recombination losses owing to short hole diffusion lengths results in a decrease in photocurrent density (Figure 3c).

To get an insight of the effect of Fe₂O₃ film thickness on the charge separation and transfer processes at the electrode electrolyte interface, Mott-Schottky (*M*-*S*) and electrochemical impedance spectroscopy (EIS) analyses are performed and are shown in Figures 3d and e, respectively. *M*-*S* plots for all three 3D electrodes exhibit positive slopes as expected for *n*-type Fe₂O₃ semiconductors.^[7,8] The flat band potential (intercept on the *x* axis) for the '3D Fe₂O₃@6 cycles' electrode is around 0.15 V (vs RHE), negatively shifted from 0.19 V (vs RHE) observed for

other two 3D electrodes, and can be attributed to the reduction of the surface Fermi level pinning effect.^[19] Moreover, the shallowest slope in the M - S plot can be observed for '3D $\text{Fe}_2\text{O}_3@6$ cycles' electrode compared to other 3D electrodes, suggesting the highest donor density for the '3D $\text{Fe}_2\text{O}_3@6$ cycles' electrode. Accordingly, carrier densities both in the dark and under light irradiation are calculated from the M - S slopes using Equation S3 (Supplementary Information) and results are tabulated in Table S2 (Supplementary Information). All of the 3D electrodes exhibit an increase in carrier densities under solar irradiation with the '3D $\text{Fe}_2\text{O}_3@6$ cycles' electrode showing the maximum enhancement (almost double, from $3.0 \times 10^{20}/\text{cm}^3$ in dark to $6.2 \times 10^{20}/\text{cm}^3$ upon solar irradiation) suggesting enhanced electronic conductivity and the values are in good agreement with those reported for other hematite based photoanodes.^[6-8,12,15,20] Such high donor densities of Fe_2O_3 films (even in dark) can be ascribed to the oxygen vacancy related defects (V_{O}) present in the Fe_2O_3 lattice, as also indicated during XPS analyses. These V_{O} sites act as shallow donor levels, thus increases the donor densities of Fe_2O_3 films, and subsequently facilitate charge transport within Fe_2O_3 film after photo-separation of charge carriers.^[10,12,21] In Figure 3e, experimental EIS data (scattered points) are fitted (solid lines) with the equivalent circuit model (shown in the inset of Figure 3d). It is to be noted that, due to high surface area and high donor concentrations in these 3D nanostructured electrodes, the space charge capacitance (C_{SC}) can be of same order of magnitude as the Helmholtz double layer capacitance (C_{H}) and therefore should not be neglected in fitting the EIS data.^[6,22] Herein the circuit, constant phase elements (CPEs) are used instead of pure capacitors in order to consider the distributed capacitances, ideal for surface charge storage in materials with disordered surface structure, like in here.^[23] As electronic processes in bulk is much faster than the charge transfer or ion diffusion processes into solution, high-frequency region of the Nyquist plot is assigned to the semiconductor resistance R_{sc} with associated CPE1 (corresponding to C_{SC}), while the low-frequency region can be represented accordingly with R_{ct} and CPE2 (that corresponds to C_{H}).^[6] The fitted values of each components are shown in Table S3 (Supplementary Information). While R_{s} for all three electrodes are almost similar (actually decreases slightly with increasing Fe_2O_3 film thickness), it is interesting to note that the R_{ct} value increases drastically with increasing Fe_2O_3 film deposition from 6 to 10 cycles, and can be attributed to the increasing Fe_2O_3 film thickness promoting charge carrier recombination and hence hindering charge transfer process. The 3D Fe_2O_3 film obtained after 6 deposition cycles has the smallest R_{ct} value, suggesting an optimum Fe_2O_3 film thickness for efficient charge transfer into electrolyte overcoming recombination losses and thus resulting in a maximum photocurrent density.

Now, to get a clearer picture of the efficacy of 3D Fe_2O_3 nanostructures over planar Fe_2O_3 , the efficiency of charge generation/separation in the bulk semiconductor ($\eta_{\text{separation}}$) and surface charge transfer efficiency (η_{transfer}) are measured using Equations S4 and S5 (Supplementary Information) after measuring the $J_{\text{photo}}-V$ curves in 1 M NaOH electrolyte with 1 M Na_2SO_3

added as a hole scavenger.^[19,20,24] The underlying idea is that, as the oxidation of SO_3^{2-} is thermodynamically and kinetically more facile than oxidation of water, therefore by measuring SO_3^{2-} oxidation photocurrent photoelectrochemical properties of the photoelectrodes can be investigated independently of water oxidation kinetics.^[24,25] Accordingly, variation of $\eta_{\text{separation}}$ and η_{transfer} with applied potentials are presented in Figure 3f. In accordance with its poor water oxidation performance, the planar Fe_2O_3 photoanode shows poor charge separation efficiency even under a high applied voltage ($\sim 10\%$ at 1.23 V vs RHE), though a good charge transfer/injection efficiency could be observed. This observation indicates that oxidation performance of planar Fe_2O_3 is mainly limited by its poor light trapping capability, resulting low yield of electron-hole pairs upon photoirradiation. Interestingly, with the incorporation of 3D Ni NCs substrate, the 3D $\text{Fe}_2\text{O}_3/\text{Ni}$ NCs photoanodes show significant enhancement in charge separation efficiency, even at lower applied voltages, and can be attributed to the enhanced light absorption efficiency by the 3D nanostructures (Figure 3b). Separation of photogenerated charges occurs at extremely low potentials (varies within 0.5 to 0.7 V vs RHE); the total charge separation efficiency raises rapidly with increasing potential and reaches a maximum value of $\sim 82\%$ (for '3D $\text{Fe}_2\text{O}_3@6$ cycles' electrode) at 1.23 V vs RHE. Meanwhile, charge transfer efficiency for the 3D electrodes increases at a faster rate compared to the planar electrode, with the 3D electrodes also showing lower onset potentials for charge transfer. Moreover, charge transfer is efficient over a wide potential range, reaching a maximum with $\eta_{\text{transfer}} \sim 88\%$ at ~ 1 V vs RHE for '3D $\text{Fe}_2\text{O}_3@6$ cycles' electrode. The enhanced charge transfer efficiency is a result of increased charge carrier lifetime and subsequent alleviation of charge recombination probability facilitated from the optimum Fe_2O_3 film thickness after 6 deposition cycles. Further increment in film thickness, much higher than the carrier diffusion length, would facilitate recombination losses and therefore results in a substantial decay in η_{transfer} , as can be observed for the '3D $\text{Fe}_2\text{O}_3@10$ cycles' electrode. It is noteworthy that the charge separation efficiency of these 3D electrodes is found to be higher as compared to the most reported hematite based photoanodes, suggesting the advantages and efficacy of the electrode design strategy reported here.^[20,26]

Transient photocurrent response of the 3D electrodes analyzed to further understand the kinetics of photogenerated charge carriers at the electrode/electrolyte interface, is recorded at a constant bias of 1 V vs RHE under intermittent solar illumination, as shown in Figure 4a. 3D Fe_2O_3 electrodes show the same kind of "spike and overshoot" photocurrent response upon photoirradiation, although the photocurrent density is significantly higher for the '3D $\text{Fe}_2\text{O}_3@6$ cycles' electrode among other 3D electrodes. For a quantitative idea about the recombination rate of photogenerated charge carriers, transient time constant (τ) is defined as time at which $\ln D = -1$, where the normalized parameter D is represented as follows [Eq. (2)].^[7,27]

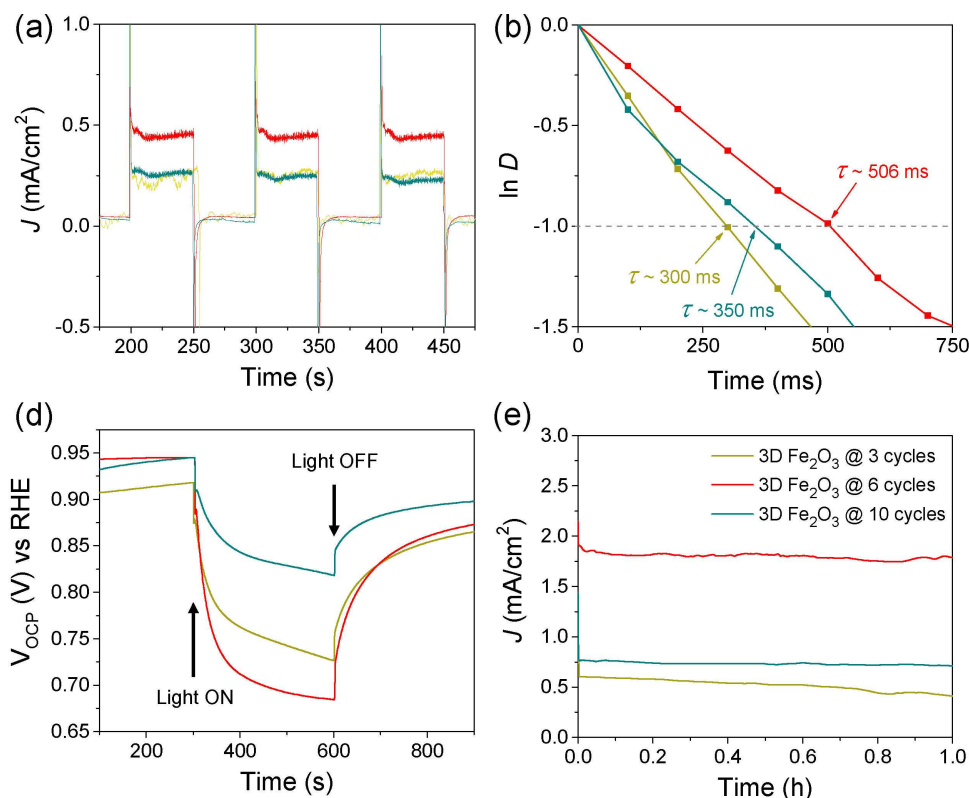


Figure 4. (a) Chronoamperometric (J vs time) curves under intermittent solar irradiation for all 3D electrodes recorded at an applied potential of 1 V vs RHE; (b) shows the normalized plots of the photocurrent-time dependence for the 3D electrodes; (c) OCP values measured for the 3D electrodes in dark and under AM 1.5G illumination; and (d) chronoamperometric (J vs time) curves of the 3D photoanodes measured at an applied potential of 1.23 V vs RHE under AM 1.5G illumination for a period of 1 h.

$$D = (I_t - I_{sat}) / (I_{in} - I_{sat}) \quad (2)$$

I_t , I_{in} and I_{sat} are the time-dependent, initial and steady state photocurrents, respectively. Shown in Figure 4b is the $\ln D$ vs *time* plots for all 3D electrodes, where it is clear that the 3D Fe_2O_3 film obtained after 6 deposition cycles exhibits largest time constant ($\tau \sim 506$ ms), suggesting suppression of its charge carriers' recombination at the electrode/electrolyte interface and hence promotion of charge transfer into electrolyte to enhance photocurrent density, which is also in accordance with the results obtained via investigation of SO_3^{2-} oxidation kinetics. The open circuit potential (OCP) measurement, as shown in Figure 4c, represents the degree of energy-band bending and can be determined by the built-in electric field at the electrode/electrolyte junction, accumulation of minority charge carriers and the extent of charge recombination.^[2,20] OCP is most positive under dark due to highest energy-band bending, which however decreases under illumination due to energy-band flattening by photogenerated carriers and can be determined by the negative shift of Fermi level in the photoanode under photoirradiation.^[2,28] Therefore, higher the degree of band bending at the electrode/electrolyte interface, more will be the electron-hole separation and charge transfer to the electrolyte. Here, it can be observed that the OCP is systematically increased with increasing Fe_2O_3 deposition from 3 to 6 cycles, suggesting an enhancement in band bending and hence

promotion of charge carrier separation followed by transfer into the electrolyte to improve PEC performance. However, OCP decreases drastically for the '3D $\text{Fe}_2\text{O}_3@10$ cycles' electrode, presumably because of the higher rate of recombination in this thick Fe_2O_3 film. A more cathodic $V_{\text{OCP-dark}}$ value observed for the 3D $\text{Fe}_2\text{O}_3@10$ cycles' electrode further indicates a relatively flattened energy-band as compared to other electrodes owing to the increased degree of charge carrier recombination probability.^[2] This analysis signifies the effectiveness of an optimum Fe_2O_3 film thickness for enlarged band bending at the electrode/electrolyte interface in achieving optimum PEC performance. Finally, a 1 h stability test of these 3D photoanodes is performed at a bias voltage of 1.23 V vs RHE under AM 1.5G solar illumination and results are shown in Figure 4d. The '3D $\text{Fe}_2\text{O}_3@3$ cycles' electrode shows slight decay in photocurrent density during the cycling test. However, '3D $\text{Fe}_2\text{O}_3@6$ cycles' and '3D $\text{Fe}_2\text{O}_3@10$ cycles' photoelectrodes exhibit photocurrents of ~ 1.8 mA/cm² and 0.75 mA/cm² which remains almost constant without showing any sign of decay during the test, suggesting excellent photostability of those Fe_2O_3 based photoanodes in aqueous electrolyte.

3. Conclusion

A facile and scalable method of fabricating hierarchical 3D Fe₂O₃ based nanostructured photoanodes is reported for their improved PEC performance as compared to planar Fe₂O₃ electrodes. In this unique design, 3D photonic Ni NC arrays not only provide improved platform for depositing Fe₂O₃ layer but also serve as efficient light-trapping centers for enhanced light absorption capability in ultrathin Fe₂O₃ layers within the whole visible region of the solar spectrum. Thickening of Fe₂O₃ film on these Ni NC arrays up to ~5 nm results in an increase in photocurrent density, which however decreases abruptly after a further increase in the film thickness. Maximum photocurrent density of ~1.86 mA/cm² vs RHE is observed for the Fe₂O₃ film obtained after 6 deposition cycles, with the efficiency of charge separation and transfer of ~82% and ~88%, respectively. This property is further supported by the prolonged transient decay time observed for the electrode. Moreover, a significant cathodic shift (~0.3 to 0.4 V) of photocurrent onset potential could also be observed for the 3D electrodes as compared to the planar photoelectrode, indicating bettered photocatalytic activity of 3D electrodes. It is envisaged that further optimization of the 3D photonic nanostructures including their spatial separation, ordering and inclusion of co-catalysts could boost the PEC performance of these 3D electrodes, thus keep scopes open for future studies.

Experimental Section

Synthesis of Ni NCs on SS Foil and Fe₂O₃ Coated Ni NCs

Large scale synthesis of Ni NC arrays was performed through an electrodeposition method using flexible stainless steel (SS) as anodic substrate and a commercial Ni plate as cathode.^[5] Before using, the substrate as well as the Ni plate were cleaned properly with a mixture solution of acetone and ethanol (1:1 vol) through ultrasonication for an hour. In aqueous electrolyte, NiCl₂·6H₂O (0.84 M) was used as Ni source, NH₄Cl (0.74 M) as crystal modifier, and H₃BO₃ (1 M) as pH buffer. The solution was kept at a temperature of 60 °C and the pH was maintained at ~4.0 by adding an appropriate amount of HCl and NaOH (10 wt% each). The electrodeposition of Ni NCs was performed at a current density of 20 mA/cm² for 500s. The solution temperature was maintained at 60 °C during electrodeposition process to avoid any Ni aggregation. After deposition, the Ni NCs coated SS foil was taken out and washed properly with a copious amount of deionized water followed by room temperature drying.

Fe₂O₃ coated Ni NC arrays were synthesized by drop casting FeCl₃ solution on the Ni NC arrays followed by drying. For this, 50 mM ethanol solution of FeCl₃ was drop casted on the Ni NC arrays and spin dried at 3000 rpm after 60s. The dried samples were subsequently heated at 100 °C for 5 min on a hot plate for enhancing particle adhesion on Ni NCs substrate. This procedure of deposition and heating is referred as one cycle and the cycle number has been varied for achieving optimum performance. Accordingly, the samples obtained after 3, 6 and 10 cycles are named as '3D Fe₂O₃@3 cycles', '3D Fe₂O₃@6 cycles', and '3D Fe₂O₃@10 cycles', respectively. Planar Fe₂O₃ samples are also prepared using similar techniques described above for comparison purpose. Finally, the samples thus prepared were annealed at 550 °C for 3 h in Ar atmosphere.

Fabrication of the Photoelectrodes for PEC Measurements

The Fe₂O₃ coated Ni NC arrays peeled off from the SS substrate was connected to an electrical wire using silver paste. Further, the back side (Ni side) and the edges of the sample, silver contact as well as the connecting wire were properly encapsulated with insulating epoxy resin keeping a certain portion in the front side (Fe₂O₃ side) of the electrode exposed for electrochemical measurements.

Structural and Morphological Characterizations

Crystallinity and morphology of the as prepared samples are investigated using X-ray diffraction (XRD, Analytical X'Pert Pro diffractometer), field emission scanning electron microscope (FES-EM, FEI Quanta-200 Mark-2), transmission electron microscope (TEM, Titan Themis), high-resolution TEM (HRTEM) and scanning TEM (STEM). The light harvesting property of the photoelectrodes is examined within UV-visible region of solar spectrum using UV-visible spectrometer (PerkinElmer LAMBDA 750). Moreover, elemental composition and chemical states of different ionic species present in samples are further investigated by energy dispersive spectroscopy (EDS), electron energy loss spectroscopy (EELS) and X-ray photo-electron spectroscopy (XPS, AXIS ULTRA) techniques.

Photoelectrochemical (PEC) Measurement Techniques

Photo-electrochemical properties of the planar and 3D electrodes are investigated through Linear Sweep Voltammetry (LSV) and chronoamperometric (*J-t*) methods in a three-electrode electrochemical cell consisting of the as-prepared samples as working electrodes, Ag/AgCl as the reference electrode, a Pt wire as the counter electrode in 1 M NaOH solution (pH~13.6), at room temperature. Nitrogen (N₂) was bubbled into the solution for an hour before PEC measurements. The electrochemical data are acquired with AutoLab PGSTAT 302 N instrument. A 300 W Xenon lamp with the AM 1.5G filter is used to illuminate the working electrodes from the front side. The scan rate for LSV scans is set at 10 mV/s. Electrochemical impedance spectroscopy (EIS) is carried out to support the PEC performance of the electrodes within the frequency range of 10 mHz to 0.1 MHz with an AC field amplitude of 5 mV. The Mott-Schottky (*M-S*) plots are obtained by performing impedance spectroscopy at a particular AC frequency of 10 kHz and then capacitances are calculated using Equation (3)

$$C = 1/2\pi Z_{im} f \quad (3)$$

where, Z_{im} is the imaginary part of the impedance at frequency f .

Notes

The authors declare no competing financial interest.

Acknowledgements

DS is grateful to the Department of Science and Technology, Government of India, for providing financial support through the INSPIRE faculty award (IFA-14 MS-32).

Conflict of Interest

The authors declare no conflict of interest.

Keywords: nanocones · ultrathin · photoanode · photoelectrochemical · water splitting

- [1] A. Fujishima, K. Honda, *Nature* **1972**, *238*, 37.
- [2] M. Zhong, T. Hisatomi, Y. Kuang, J. Zhao, M. Liu, A. Iwase, Q. Jia, H. Nishiyama, T. Minegishi, M. Nakabayashi, N. Shibata, R. Niishiro, C. Katayama, H. Shibano, M. Katayama, A. Kudo, T. Yamada, K. Domen, *J. Am. Chem. Soc.* **2015**, *137*, 5053.
- [3] Y. Zeng, H. Li, J. Luo, J. Yuan, L. Wang, C. Liu, Y. Xia, M. Liu, S. Luo, T. Cai, S. Liu, J. C. Crittenden, *Appl. Catal. B* **2019**, *249*, 275.
- [4] Y. Qiu, S.-F. Leung, Q. Zhang, B. Hua, Q. Lin, Z. Wei, K.-H. Tsui, Y. Zhang, S. Yang, Z. Fan, *Nano Lett.* **2014**, *14*, 2123.
- [5] J. Li, Y. Qiu, Z. Wei, Q. Lin, Q. Zhang, K. Yan, H. Chen, S. Xiao, Z. Fan, S. Yang, *Energy Environ. Sci.* **2014**, *7*, 3651.
- [6] F. Le Formal, N. Tétreault, M. Cornuz, T. Moehl, M. Grätzel, K. Sivula, *Chem. Sci.* **2011**, *2*, 737.
- [7] A. K. Singh, D. Sarkar, *Nanoscale* **2018**, *10*, 13130.
- [8] Y. Ling, G. Wang, D. A. Wheeler, J. Z. Zhang, Y. Li, *Nano Lett.* **2011**, *11*, 2119.
- [9] K. Sivula, F. L. Formal, M. Grätzel, *Chem. Mater.* **2009**, *21*, 2862.
- [10] D. Sarkar, A. Shukla, D. D. Sarma, *ACS Energy Lett.* **2016**, *1*, 82.
- [11] C. Liu, J. Ma, H. Chen, *RSC Adv.* **2012**, *2*, 1009.
- [12] Y. Ling, G. Wang, J. Reddy, C. Wang, J. Z. Zhang, Y. Li, *Angew. Chem. Int. Ed.* **2012**, *51*, 4074.
- [13] D. Sarkar, G. G. Khan, A. K. Singh, K. Mandal, *J. Phys. Chem. C* **2012**, *116*, 23540.
- [14] T. Fujii, F. M. F. de Groot, G. A. Sawatzky, F. C. Voogt, T. Hibma, K. Okada, *Phys. Rev. B* **1999**, *59*, 3195.
- [15] I. Cesar, K. Sivula, A. Kay, R. Zboril, M. Grätzel, *J. Phys. Chem. C* **2009**, *113*, 772.
- [16] A. M. Jubb, H. C. Allen, *ACS Appl. Mater. Interfaces* **2010**, *2*, 2804.
- [17] D. Bersani, P. P. Lottici, A. Montenero, *J. Raman Spectrosc.* **1999**, *30*, 355.
- [18] D. Sarkar, M. Mandal, K. Mandal, *ACS Appl. Mater. Interfaces* **2013**, *5*, 11995.
- [19] S. Wang, P. Chen, J.-H. Yun, Y. Hu, L. Wang, *Angew. Chem. Int. Ed.* **2017**, *56*, 8500.
- [20] F. Li, J. Li, F. Li, L. Gao, X. Long, Y. Hu, C. Wang, S. Wei, J. Jin, J. Ma, *J. Mater. Chem. A* **2018**, *6*, 13412.
- [21] D. Sarkar, S. Das, S. G. B. Pal, H. Rensmo, A. Shukla, D. D. Sarma, *J. Electrochem. Soc.* **2017**, *164*, A987.
- [22] J. Wielant, V. Goossens, R. Hausbrand, H. Terryn, *Electrochim. Acta* **2007**, *52*, 7617.
- [23] T. Brezesinski, J. Wang, R. Senter, K. Brezesinski, B. Dunn, S. H. Tolbert, *ACS Nano* **2010**, *4*, 967.
- [24] T. Yao, R. Chen, J. Li, J. Han, W. Qin, H. Wang, J. Shi, F. Fan, C. Li, *J. Am. Chem. Soc.* **2016**, *138*, 13664.
- [25] L. Zhou, C. Zhao, B. Giri, P. Allen, X. Xu, H. Joshi, Y. Fan, L. V. Titova, P. M. Rao, *Nano Lett.* **2016**, *16*, 3463.
- [26] a) F. Tao, G. Yongsheng, C. Songhua, Z. Ningsi, H. Yingfei, Z. Shiyang, L. Zhaosheng, Z. Zhigang, *Nanotechnology* **2017**, *28*, 394003; b) J. Huang, G. Hu, Y. Ding, M. Pang, B. Ma, *J. Catal.* **2016**, *340*, 261; c) L. Wang, N. T. Nguyen, X. Huang, P. Schmuki, Y. Bi, *Adv. Funct. Mater.* **2017**, *27*, 1703527.
- [27] D. Tafalla, P. Salvador, R. M. Benito, *J. Electrochem. Soc.* **1990**, *137*, 1810.
- [28] A. Zaban, M. Greenshtein, J. Bisquert, *ChemPhysChem* **2003**, *4*, 859.

Manuscript received: September 27, 2019
Accepted manuscript online: October 14, 2019
Version of record online: October 28, 2019